Linear and nonlinear Biot waves in a noncohesive granular medium slab: Transfer function, self-action, second harmonic generation

J-B. Legland, V. Tournat, O. Dazel, and A. Novak
LAUM, CNRS, Université du Maine, Avenue O. Messiaen, 72085 Le Mans, France

V. Gusev
IMMM, CNRS, Université du Maine, Avenue O. Messiaen, 72085 Le Mans, France

(Received 27 October 2011; revised 10 April 2012; accepted 11 April 2012)

Experimental results are reported on second harmonic generation and self-action in a noncohesive granular medium supporting wave energy propagation both in the solid frame and in the saturating fluid. The acoustic transfer function of the probed granular slab can be separated into two main frequency regions: a low frequency region where the wave propagation is controlled by the solid skeleton elastic properties, and a higher frequency region where the behavior is dominantly due to the air saturating the beads. Experimental results agree well with a recently developed nonlinear Biot wave model applied to granular media. The linear transfer function, second harmonic generation, and self-action effect are studied as a function of bead diameter, compaction step, excitation amplitude, and frequency. This parametric study allows one to isolate different propagation regimes involving a range of described and interpreted linear and nonlinear processes that are encountered in granular media experiments. In particular, a theoretical interpretation is proposed for the observed strong self-action effect. © *2012 Acoustical Society of America*.
[http://dx.doi.org/10.1121/1.4712020]

PACS number(s): 43.25.Dc, 43.20.Gp, 43.25.Ed, 43.25.Zx [ANN] Pages: 4292–4303

I. INTRODUCTION

Grains and grain assemblages (granular media) are involved in a large number of industrial and natural processes[1,2] and are the subject of intense fundamental research efforts from the properties of a single contact at the nanoscale to collective effects involving thousands of particles.[3–8] The interest in these media are particularly shared among researchers in fluid mechanics, contact mechanics, soft matter physics, geophysics, and acoustics. For most of the studied processes, both static and dynamic, the nature of the saturating fluid is a determinant property of the medium. For instance, the fluid can strongly modify the contact properties,[9,10] leading to completely different static and dynamic behaviors of the packings in comparison with the case of the grains in vacuum. Even a small amount of humidity can induce strong differences in contact properties and packing elasticity.[11,12]

The acoustic properties can also be completely modified depending on the saturating fluid, independently of the contact property influence. It is well-known that the fluid properties play an important role on the propagation of sound in porous media, in particular in the context of Biot waves.[13–15] Numerous studies have been carried out and specific models derived for marine sediments, i.e., water saturated granular media with applications to sea-floor sounding.[16–18] When the ratio of skeleton-to-fluid acoustic impedances is modified (by the elasticity or density modification), the coupling between acoustic energy in the solid skeleton and acoustic energy in the fluid is modified. Such constitutive parameters as the fluid flow resistivity, or the fluid compressibility, for instance, are fluid dependent. These parameters can also depend on the geometry of the porous sample. In particular, for disordered granular packings composed of the same spherical beads, the geometrical parameters of the packing depend mainly on the bead diameter d and the compacity Φ (or packing fraction, defined as the volume occupied by the beads over the total volume of the packing including the saturating fluid).[19] For instance, the bead diameter d plays a role on the acoustic parameters of the "equivalent fluid,"[15,20] through the diameter dependence of the flow resistivity $\sigma \propto d^{-2}$ or viscous characteristic length $\Lambda \propto d$.

There are numerous studies of acoustic wave propagation through the solid skeleton of granular packings neglecting the influence of the saturating air.[9,21–29] Also, there exist several reported results on the acoustic propagation through granular media considered as "equivalent fluids," i.e., without considering acoustic motion of the solid skeleton.[20,30–32] However, only a few articles report results where the coupling of waves in the solid skeleton of granular packings and the saturating air takes place. In Ref. 33, there have been observations of energy transfer from the solid skeleton (the beads and their contacts) to the saturating air in a nonlinear self-demodulation experiment in granular media. In this work,[33] the excited wave packet was launched in the medium and self-demodulated in the highly nonlinear solid skeleton of the packing. With a microphone, it was possible to detect the self-demodulated signal in air after energy transfer from solid skeleton to air. This process was found to be dependent on the static pressure applied on the grains. The influence of bead diameter and compaction step has not been studied, however.

 0001-4966/2012/131(6)/4292/12/$30.00

Recently, laboratory and numerical studies of the compaction process were performed in order to solve basic scientific questions that are still open,[34] and also to provide efficient protocols for producing high density, rigid, and stable granular packings in practical applications.

While the most used experimental parameter characterizing the compaction process is the compacity Φ of the packing, the same value of Φ could correspond to granular media in rather different mechanical states because of different statistical distributions of the inter-grain contact interaction forces.[34–36] Thus it is obvious that for both industrial and fundamental studies, the monitoring of the granular packing elasticity during compaction is relevant and of primary importance. The measurements of linear mechanical properties of the granular packing provide information mainly on average (effective) characteristics of the contact forces distribution,[25,37] which, however, is still insufficient for a unique identification of the mechanical state. The simplest theoretical arguments[24] indicate that the weak contacts could provide a dominant contribution to nonlinear mechanical properties of the granular media. It has been recently proven experimentally that nonlinear acoustic methods (based on monitoring of the modification of the acoustic field spectrum with increasing field amplitude) provide complementary information on the statistical distribution of the weak intergrain forces, which is inaccessible by linear acoustic methods.[37] However, in order to achieve such needed accurate acoustic probing of the granular packing elasticity, one has to understand the effect of the saturating air on the linear and nonlinear acoustic responses of these media.

In this work, we present an experimental parametric study of the acoustic transmission through a granular medium slab. We are able, with our experimental setup, to vary the compacity of the packing from $\Phi \simeq 0.58$ to $\Phi \simeq 0.63$, the bead diameter ($d \simeq 0.7$, 1.4, and 2 mm, respectively), and the excitation amplitude by two orders of magnitude. Linear transmission as well as second harmonic generation and self-action effects are analyzed. Results are compared to theoretical modeling of Biot wave propagation and second harmonic Biot wave generation.[38] Explanation for the observed strong nonlinear self-action effect is provided.

II. EXPERIMENTAL SETUP AND METHODS

A. Setup and samples

Our samples consist of random packing of glass beads contained in a rectangular based box of height 100 mm and lateral size $L \times \ell = 80 \times 80$ mm (Fig. 1). The initial configuration is obtained by quickly pouring the beads in the container, with a metallic grid (5×5 mm square holes formed with 0.5 mm in diameter metallic wires) placed inside at the bottom. Then, the grid is slowly moved through the medium up to the top of the container. This provides an initial compacity value $\Phi \simeq 59\%$ reproducible for a given bead sample within 0.5%. In order to mechanically excite the granular column, a shaker delivering discrete vertical pulses, or "taps," with a 1 Hz repetition rate, is placed below the container. Each shaker pulse consists of a sinus period of frequency 60 Hz, monitored by an accelerometer mounted on the

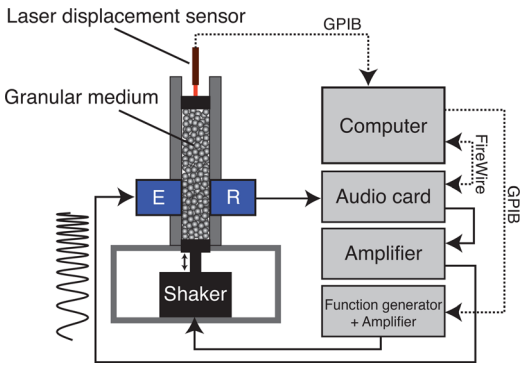

FIG. 1. (Color online) Experimental setup. "E" and "R" are the piezo-emitter and the piezo-receiver. The experiment is computer controlled, with packing volume measure, solicitation by mechanical taps via the low-frequency shaker, and acoustic probing.

membrane supporting the granular sample. The typical maximum acceleration used for each tap is $a \simeq 3g$ at the bottom of the granular column. The measurement of the packing height relative variations, leading to a measure of the compacity change, is achieved through a laser displacement sensor with a precision better than 1 μm. Relative change in packing compacity is then measured with a precision of 0.05%. The static pressure applied by gravity on the granular packing at the location of the acoustic probing is of the order of 1 kPa.

Two piezoelectric transducers embedded in the vertical walls of the container constitute a resonator for the low frequency acoustic waves launched in the granular medium. The frequency of the fundamental resonance for the longitudinal mode is $f_0 = c_0/2L \simeq 1$ kHz for the rigid boundary conditions of our configuration where the linear sound speed c_0 corresponds to the longitudinal wave speed in the solid matrix. At the initial stage of compaction c_0 was estimated to be $\sim$160 m/s from the first resonance frequency of the granular slab. To ensure that the lowest observed resonance is the one of the first order, we also estimated c_0 by pointing the arrival time of a pulse front which propagated through the 8 cm distance between the transducers. Considering the acoustic attenuation and the 8 cm propagation length between the transducers, it is only possible to observe the few first resonances of the granular slab, below 5 kHz, and most of the studied processes, over 5 kHz, take place for one-way progressive waves.

B. Data analysis and signal processing

The method implemented here allows within one single measurement of time length $T \simeq 2$ s to characterize the nonlinear system in both amplitude and phase, not only for the fundamental harmonic as usual with a spectrum analyzer, but also for nonlinearly generated higher harmonics.[39] Consequently, it allows one to estimate the transfer of energy, not only on the first harmonic, but also on higher harmonics. Energy transfer to higher harmonics is estimated through the so-called higher-order frequency response functions (FRFs).[39,40] This method also provides estimation of the phase spectra of the higher-order FRFs.

The analysis procedure is divided into two parts. First, the input swept-sine signal $s(t)$ is generated to excite the nonlinear system (the granular slab here) whose response $y(t)$ is synchronously recorded. Next, the convolution between the output $y(t)$ and an inverse filter is calculated. The use of the inverse filter for separating higher-order components was proposed in Ref. 41, and corresponds to the time-reversal of the excitation signal equalized with a slope of -6 dB/oct (time-reversal mirror plus whitening filter). When convolving the output $y(t)$ and the inverse filter, the result yields in setting of nonlinear impulse responses. They can be easily separated by windowing and their Fourier transforms are equal to the higher-order FRFs.

Here we make use of only the two first order FRFs since the acquisition sampling frequency is limited to 192 kHz. The second harmonic wave is consequently analyzed up to a maximum frequency of excitation of 48 kHz. All results in the following are shown up to a 45 kHz fundamental excitation frequency.

III. EXPERIMENTAL RESULTS

In the following, we report on the characteristic effects that have been observed along a series of parametric experiments on controlled granular slabs. The studied parameters are the bead size, the compaction step, and the excitation amplitude. The frequency is swept from 500 Hz to 45 kHz in the presented transfer functions. We first analyze the fundamental transfer function and provide interpretations based on a previously developed model.[38,42] Then, we report the observation of second harmonic generation and strong self-action effect. Interpretations for the observed effects are then proposed and discussed.

A. Analysis of the transfer function

1. Characteristic frequency regions of the transfer function

In Fig. 2, the experimental acoustic transfer function of a granular slab is compared to theoretical results of the

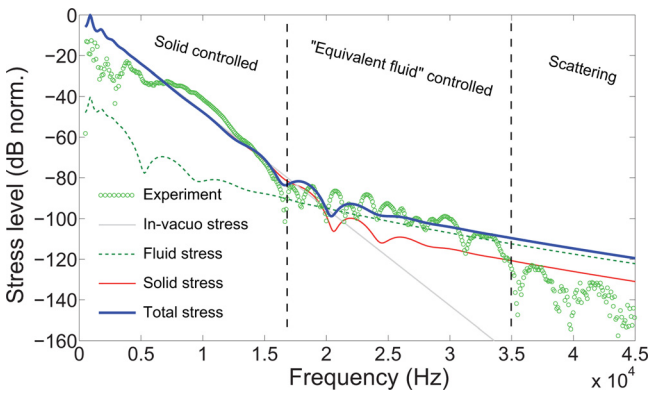

FIG. 2. (Color online) Acoustic transfer function of an 8 cm thick granular medium slab composed of 0.7 mm in diameter glass beads. A compaction process with 5000 taps was applied. The experimental frequency response is corrected by the emitter and receiver sensitivities. All the curves are normalized to the maximum of the theoretical total stress. Parameters of the model for the fluid are fixed by the air properties and the bead diameter (Ref. 38). The longitudinal elastic modulus of the solid skeleton is taken as $E = 30 \times 10^6(1 + 0.33i)$ Pa in the modeling.

modeling of Biot waves from the model in Ref. 38 and briefly described in the following. The value taken for the longitudinal elastic modulus of the solid skeleton is adjusted to obtain a qualitative agreement with the experimental curve and is consistent with the wave velocity estimation. Note that due to the medium complex behavior, one cannot expect a quantitative agreement over the whole frequency range with a single parameter adjustment. Also, a satisfying agreement is obtained with slightly different values up to a few tens of percent change. In the studied configuration, with a longitudinal acoustic wave generated on one side of the granular slab and one detected on the other side, the geometry is considered one-dimensional. This assumption is reasonable for frequencies above $\sim$5 kHz for which the acoustic beam diffraction length becomes larger than the propagation distance, i.e., local plane waves travel through the medium. Consequently, only two Biot modes exist, involving both motion of the solid skeleton and saturating fluid. These two propagation modes contribute to the experimentally detected total stress on the detection side. Theoretically and numerically, it is possible to isolate two different contributions to the detected total stress σ_t: the stress in the solid skeleton σ_s (denoted by solid stress in Fig. 2) and the acoustic pressure in the saturating fluid P_f or fluid stress $\sigma_f = -P_f$. These acoustic stresses verify

$$\sigma_t = \sigma_s - P_f. \tag{1}$$

Solutions of the acoustic problem with longitudinal Biot waves in the one-dimensional slab are given in the form[38]

$$u^s = [A_1 \sin(k_1 x) + A_2 \sin(k_2 x) + B_1 \cos(k_1 x) + B_2 \cos(k_2 x)]e^{j\omega t}, \tag{2}$$

$$u^t = [\mu_1 A_1 \sin(k_1 x) + \mu_2 A_2 \sin(k_2 x) + \mu_1 B_1 \cos(k_1 x) + \mu_2 B_2 \cos(k_2 x)]e^{j\omega t}, \tag{3}$$

where u^s is the solid displacement and u^t the total displacement (a combination of the solid and fluid displacement), x is the coordinate in the propagation direction, t is the time, and ω is the cyclic frequency.[43] The terms A_i, B_i, μ_i, and k_i are, in general, frequency dependent and can be expressed using physical, mechanical, and geometrical parameters of the medium such as the air flow resistivity, the characteristic viscous and thermal length, the tortuosity, the solid skeleton longitudinal elastic modulus, the air, and solid densities. The whole set of parameters and their expressions for granular media are given in Ref. 38. Rigid boundary conditions are considered, i.e., $u^s = u^t = 0$ at the detection face of the slab and $u^s = u^t = u_0(\omega)\cos(\omega t)$ for the excitation boundary [$u_0(\omega)$ is the frequency dependent displacement sensitivity of the emitter]. The stresses associated with the displacements in Eqs. (2) and (3) are

$$\sigma_s = E\frac{\partial u^s}{\partial x}, \tag{4}$$

$$\sigma_f = -P_f = M\frac{\partial u^t}{\partial x}, \tag{5}$$

where E is the solid skeleton longitudinal elastic modulus and M the frequency dependent equivalent compressibility of the air [the fluid compressibility of the "equivalent fluid model" defined by Eqs. (B1)–(B6) in Ref. 38].

In Fig. 2, it is possible to split the acoustic transfer function into three characteristic frequency bands. In the lowest frequency band, the solid stress dominates over the fluid pressure and is the main contribution to the total stress. The acoustic transfer function depends mainly on the solid skeleton properties. In the middle frequency band, the fluid pressure becomes the main contribution to the total stress. The medium can, in this case, be considered as an "equivalent fluid," with acoustic properties independent of the solid elasticity (the wave energy propagates in the saturating fluid mainly and independently of the solid). The third frequency band, at higher frequencies, exhibits deviation of the model compared to the experimental total stress. We believe that the long wavelength (homogenization) limit is not fulfilled anymore and scattering effects in the equivalent fluid may occur.

2. Discussion on the cut-off frequency

The characteristic frequency where a transition occurs from solid stress controlled to equivalent fluid controlled regimes has already been defined as a cut-off frequency f_c.[38] In the vicinity of this cut-off frequency, the solid stress and fluid pressure have comparable magnitudes which enable interferences often leading to a nonmonotonous frequency dependence of the total stress with local minima and maxima. This behavior is observed for both the experimental and the theoretical total stresses in Fig. 2.

Note that in principle, the transition frequency f_c from solid stress controlled to equivalent fluid controlled regimes is a nontrivial function of the bead size, wave attenuation in both solid and fluid, propagation distance, compacity, static stress, etc. A theoretical accurate description of f_c is beyond the scope of the present article. However, due to the strong drop in solid stress level just before the transition between the two regimes, it appears that the main effect controlling f_c is the attenuation by scattering of the stress wave in the solid skeleton (this point is discussed in Sec. III C). As a consequence, f_c is mostly determined by the scattering properties of the stress wave in the solid skeleton.

Note also that this cut-off frequency f_c could be compared to the cut-off frequency of a one-dimensional granular chain corresponding to the limit of the Brillouin zone of the lattice $F_c = c_0/(\pi d)$, where c_0 is the low frequency limit of the wave velocity in the system.[44–46] For the low frequency wave velocities observed in the disordered granular slab that range between $c \simeq 100$ m/s and $c_0 \simeq 160$ m/s, the estimated one-dimensional chain cut-off frequency is estimated as $F_c \simeq 45$–72 kHz for $d = 0.7$ mm and $F_{c_0} \simeq 16$–25 kHz for $d = 2$ mm. These values, suitable for an ordered one-dimensional granular system, over-estimate the values of f_c observed here for a disordered packing by a factor of 3–4, but are not orders of magnitude different suggesting that similar wave processes could take place in both cases. This statement is supported by the fact that the presence of disorder (both geometrical and in the contact forces) produces wave scattering at wavelengths larger than the bead diameter,[47] i.e., at lower frequencies than the estimated F_c.

As an estimate, the observed cut-off frequency $f_c \simeq 16$ kHz in Fig. 2 corresponds to a product $k_s d \simeq 0.44$ between the wavenumber in the solid skeleton k_s and the bead diameter d (with a wave velocity $c_0 \simeq 160$ m/s). In Fig. 3, at the cut-off frequencies $f_c \simeq 10$ kHz and 12 kHz observed for the two other bead sizes $d = 1.4$ mm and 2 mm, our estimates give $k_s d \simeq 0.66$ and $k_s d \simeq 0.78$, respectively. One should note that these three $k_s d$ values even if they are of the same order of magnitude are not equal. Consequently, the experimental cut-off frequency, although mainly attributed to the strong attenuation by scattering in the solid skeleton, is not a trivial function of the parameter k_d and depends on several other medium parameters (fluid properties, bead diameter, static pressure, compacity).

The expected scattering at the limit between the middle and the third characteristic frequency bands of the transfer function occurs at ~35 kHz in Fig. 2. By estimating the equivalent fluid wave velocity using its high frequency asymptotic limit $c_a/\sqrt{\alpha_\infty} \simeq 287$ m/s, where $c_a \simeq 340$ m/s is the wave velocity in air and $\alpha_\infty \simeq 1.4$ is the tortuosity,[20,38] the product between the equivalent fluid wavenumber k_a and the bead diameter d is estimated at the transition frequency of 35 kHz to be $k_a d \simeq 0.54$. It is comparable to the products $k_s d$ at the cut-off frequency between the first (solid controlled) and second (equivalent fluid controlled) characteristic frequency bands.

We also found that the process of Rayleigh scattering producing the observed transmission drop close to the characteristic frequency f_c for the solid stress wave does not saturate right above f_c. In Ref. 48, simulations on the elastic energy transport through random loose rigid sphere packings have been carried out in the context of thermal transport in glasses. The normal modes of vibrations of packings of spheres interacting through a one-sided harmonic potential (just repulsion forces) have been calculated for different geometrical configurations close to jamming. From the normal modes of vibration, the energy diffusivity is obtained as a function of frequency. One of the conclusions about the

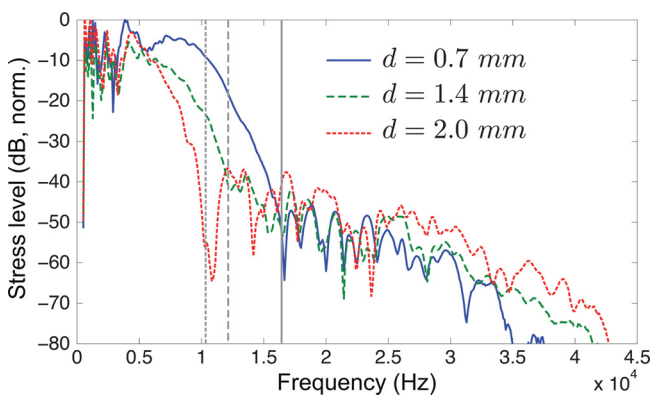

FIG. 3. (Color online) Received acoustic stress levels at the fundamental frequency (first order FRF) for three granular samples composed of different bead diameters d. All three samples are compacted with 5000 taps. Vertical lines show estimates of the cut-off frequencies f_c for each FRF. Curves are normalized to the maximum of the first order FRF for $d = 0.7$ mm.

elastic wave scattering is that there exists a characteristic frequency f_d of transition between a weak (Rayleigh) scattering regime and a strong scattering regime (with smaller frequency dependence). For the longitudinal waves considered here, and using the simulation results of Fig. 2 in Ref. 48, we derive the following formula:

$$f_d \simeq \frac{n}{2\pi}\frac{c_0}{d}, \tag{6}$$

where $n \simeq 2-3$ is a pre-factor deriving from d_0 in Ref. 48 and from the disordered character of the packing, and c_0 is the longitudinal wave velocity in the solid skeleton. For $c_0 = \sqrt{E/\rho} \simeq 160\,\text{m/s}$, $d = 0.7\,\text{mm}$, and $n \simeq 2$, we obtain $f_d \geq 70\,\text{kHz}$. The fact that the estimate of f_d is well above f_c shows that the transition observed in Fig. 2 at $\sim$16 kHz is not associated to a transition from weak to strong scattering regimes but rather from the dominance of weak scattering of the solid stress wave (leading to the strong drop in amplitude as a function of frequency) to the dominance of the fluid stress contribution.

3. Elastic parameters of the solid frame

Due to the frequency scale chosen in Fig. 2, the resonances are not clearly seen. Still, they exist for both experimental and theoretical total stresses. These resonances in the solid part of the granular medium can be used for characterization of the elastic properties of the packing as in Ref. 37. The evaluation of the longitudinal elastic modulus of the solid skeleton was obtained through the first resonance frequency measurement. Its frequency dependence and imaginary part have to be found. The other constitutive parameters of the model developed in Ref. 38 are known *a priori* from the bead size, bead material, and packing geometry.

For the model presented in Fig. 2, the longitudinal elastic modulus of the solid skeleton is taken in the form

$$E = E_0(1 + i\eta). \tag{7}$$

Experimental observations in the solid-controlled region can be reasonably well-fitted assuming the attenuation proportional to frequency, i.e., a constant value $\eta = 0.33$, already observed in various granular media.[49] The derived value for the real part of the elastic modulus is $E_0 = 30\,\text{MPa}$. This value is realistic considering that it provides a longitudinal wave velocity in the solid skeleton of $c_0 \simeq 140$ m/s.

It is important to note here that only the elastic parameter of the solid skeleton is adjusted; all the other parameters are being included in the model without optimization. The behavior of the acoustic transfer function in the middle frequency band is well-captured by the model, in particular the oscillating behavior and the slowly decreasing trend as a function of frequency. This observation, among others presented in the following, confirms the predominant role of the fluid in this frequency range: The granular packing saturated by air behaves as an equivalent fluid. In the low frequency region, however, the agreement between theory and experiment is only qualitative—existence of slab resonances and decrease of the transfer function with frequency. More elaborated models for the solid skeleton elasticity are certainly needed, but there is a lack of information on the frequency dependence of both the real and imaginary parts of the elastic modulus. In Fig. 4 and in the discussion, a model for the frequency dependent imaginary part is proposed and discussed. Besides, the acoustic transfer function is strongly dependent on the compaction step, the applied static pressure, the acoustic excitation level, and the bead size, as it will be presented in the following sections. Consequently, an accurate model optimization of the solid skeleton behavior is, at the moment, illusory, but the present work could contribute to building such a model.

B. Effect of the compaction

The effect of the compaction level is shown in Fig. 5 where the received acoustic level is plotted as a function of frequency for two different amounts of applied taps. The curve "after compaction" representing the acoustic stress level received through a compacted granular slab corresponds to the same data as the acoustic transfer function of Fig. 2 (with a different correction of the transducer sensitivity). This sensitivity correction, leading to the presentation of the real received acoustic level as a function of frequency (and not the acoustic transfer function) is adopted now because it is more suitable for analyzing nonlinear effects.

In Fig. 5, the main effect of the compaction process occurs below the cut-off frequency of $f_c \simeq 16\,\text{kHz}$ separating the low and middle frequency regions discussed above for Fig. 2. Consequently, the compaction process influences predominantly the solid skeleton elasticity through the increase of compacity and possibly the increase in static stress between the beads and the container walls. Note that from other experiments in the same configuration,[37] the monitoring of the first resonance frequency of the granular slab submitted to a compaction process shows that the longitudinal velocity increases. Thus, the longitudinal elastic modulus increases much faster than the density (by only a few percent) along a compaction process. This is compatible with an increase of the cut-off frequency (due to the increase of

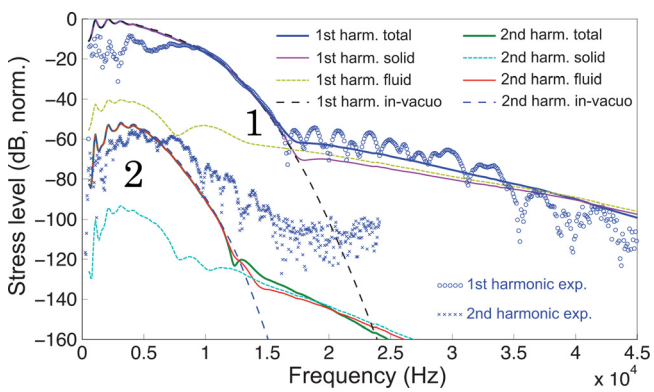

FIG. 4. (Color online) Received acoustic stress levels for the fundamental (1st harmonic denoted by 1) and the 2nd harmonic (denoted by 2) components. Glass beads are 0.7 mm in diameter and 5000 taps have been applied (same data as in Fig. 2). The received amplitudes have been corrected by the receiver sensitivity only (which is different from Figs. 2 and 5), and all the curves are normalized to the maximum of the theoretical total stress.

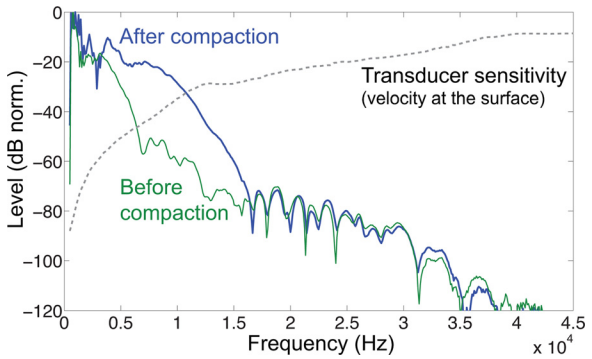

FIG. 5. (Color online) Acoustic transfer function for two different medium densities obtained before compaction ($\Phi \simeq 0.59$) and after compaction (5000 taps, $\Phi \simeq 0.63$). Glass beads are 0.7 mm in diameter. The same sensitivity correction as in Fig. 2 is applied and curves are normalized to the maximum of the curve "after compaction."

wave velocity and wavelength) as observed in Fig. 5, from $f_c \simeq 7$ kHz to $f_c \simeq 16$ kHz. The characteristic frequency f_c is determined here by pointing the first local minimum of the experimental transfer function after the strong drop in amplitude.

In the middle frequency region, the few percent change in compacity (or, equivalently, on porosity) due to compaction has a weak influence on the received acoustic stress. The equivalent fluid parameters of the medium that depend on compacity and bead size are only slightly modified. In this region, the received acoustic stress is independent of the solid skeleton elasticity change, which confirms the equivalent fluid regime predominance. It is interesting to notice that the compaction process can provide for the $\sim$6 kHz to $\sim$12 kHz frequency band, a 40dB difference in the transmitted acoustic stress level (a factor 100 for the amplitude or 10^4 for the acoustic energy).

C. Second harmonic generation process

The second harmonic generation process is now analyzed over a wide frequency range thanks to the method presented in Sec. II B. Similar to Fig. 2, the acoustic stress level is presented as a function of frequency in Fig. 4. The same data as in Fig. 2 is used for the fundamental (or 1st harmonic) component. Here, additionally, the acoustic stress level of the second harmonic is presented. The frequency axis in Fig. 4 represents the frequency of the fundamental wave. In other words, the second harmonic level presented at the (fundamental) frequency of 10 KHz corresponds to the second harmonic level at 20 kHz. The noise level for the experimental results is of the order of -100 dB in this experiment.

In Fig. 4, the experimental FRFs of first and second order are compared to the model[38] using the following model for the solid skeleton elasticity:

$$E = E_0\left\{[(\omega/\omega_c)/\arcsin(\omega/\omega_c)]^2 + i(\eta_1/\omega + \eta_2 + \eta_3\omega^3)\right\} \quad (8)$$

with $E_0 = 40$ MPa, $\eta_1 = 0.5$e3 rad/s, $\eta_2 = 0.25$, and $\eta_3 = 1.5$ e-16 (rad/s)$^{-3}$. $\omega_c = 2c/d$ is the cut-off cyclic frequency of the one-dimensional granular chain.[46] For $\omega \ll \omega_c$, the real part of E tends to E_0 as in the model (7). The term η_2 in the imaginary part is similar to the term η in Eq. (7).

The weak agreement observed at the lowest frequencies can be associated with the role of diffraction of the acoustic beams in experiments leading to a deviation from the ideal one-dimensional geometry as considered in the model. Consequently, the acoustic level is overestimated by the model which does not capture the acoustic energy spreading by diffraction. The term η_1/ω plays a role for small ω and attempts to depict, in a heuristic way, the observed plateau at low frequencies possibly associated with this effect of geometrical attenuation by acoustic beam diffraction. Note that it would be possible to precisely take into account the frequency dependent diffraction effect on the FRF, but it is not the main goal here, and it would not be compatible with the one-dimensional Biot model.

The term $\eta_3\omega^3$ provides attenuation due to Rayleigh scattering and allows for an accurate fit of the drop in transmission observed between $\sim$10 kHz and $\sim$18 kHz in Fig. 4. We consequently hypothesize that the rapid decrease observed between $\sim$10 kHz and $\sim$18 kHz is due to scattering of the waves in the disordered solid skeleton. This idea is compatible with the compaction effect observed in Fig. 5, which tends to increase the acoustic wavelength and decrease the level of disorder in the medium, providing in turn a lower attenuation by scattering for a frequency in the considered range. This idea is also compatible with the strong self-action effects for this frequency range as reported in Sec. III E. Note that physically, when frequency increases, the Rayleigh type frequency dependent attenuation in the solid should saturate at some point, as discussed in Sec. III A 2. However, this transition is expected to occur above frequency $f_d \sim 70$ kHz, here. Moreover, when the solid stress contribution is much less than the fluid stress one, the role of attenuation in the solid has a negligible effect on the total stress.

Qualitatively, the observed second harmonic stress level is similar to the one from the model. The only adjusted parameter is the parameter of quadratic nonlinearity of the solid. Modification of this parameter provides only a constant shift in amplitude of the second harmonic at all frequencies. A frequency dependence of this parameter could in principle be introduced and could explain the discrepancy above 10 kHz. However, we think that it would be too hypothetical because the observed discrepancies can also be attributed to other effects (deviation from the elastic quadratic nonlinearity, for instance).

For a single contact between two beads, a Taylor expansion of the stress-strain relationship in the limit of a very small acoustic amplitude in comparison to the static precompression provides a parameter of quadratic nonlinearity

$$\beta = \frac{1}{4\varepsilon_0}, \quad (9)$$

where ε_0 is the static deformation of the contact (here taken positive for compression).[24] For an estimated static stress σ_0

$\simeq$ 750 Pa and considering an elastic modulus $E_0 = 30$ MPa, the contact average static deformation is $\varepsilon_0 \simeq 2.5 \times 10^{-5}$ and the parameter of quadratic nonlinearity is $\beta \simeq 10^4$. In Fig. 4, the value found to correctly fit the second harmonic wave amplitude is adjusted to $\beta = 3 \times 10^4$, larger than the estimated value. The discrepancy, corresponding to a factor of 3, can be attributed to the uncertainty of the second harmonic level fit, which can easily reach ± 5 dB (see Fig. 4). Also, the estimation is based on the average static deformation while there exists a distribution of contact deformations including contacts with weaker than average static deformations and exhibiting consequently higher nonlinearity.[24,50,51] So, there is an uncertainty on the value of β adjusted with experiments, and the estimated value of β using the average static deformation may under-estimate β in the case of a distribution of static deformations. Still, the two parameters of quadratic nonlinearity derived differently are of the same order of magnitude and provide a useful estimation.

D. Influence of the bead diameter

Effects of the bead diameter on the first and second order FRF are now analyzed. In Fig. 3, the first order FRFs obtained for three granular samples composed of different bead diameters are plotted. The cut-off frequencies f_c between the solid controlled region and the fluid controlled region are estimated visually. They tend to increase with decreasing bead diameter as expected from the theory when attenuation in the solid skeleton due to scattering is taken into account [as in Eq. (8)]. This observation also confirms the interpretation that the fast transmission drop in the solid skeleton is related to scattering as discussed earlier in Sec. III A 2. The maximum transmitted acoustic stress is observed to be similar for the different bead diameters showing that dissipation in the solid skeleton at frequencies lower than 5 kHz is not drastically different. However, for frequencies larger than 5 kHz and up to the cut-off frequencies f_c, large level differences are observed depending on the sample bead size. This observation could be put in relation with the modification of the FRF by a compaction process as shown in Fig. 6, where the cut-off frequency increases with the compaction step. It could be concluded that compaction, by increasing the average number of contacts (providing a higher density of acoustic path through the packing), and certainly increasing static pressure (by mobilizing more and more friction with the container walls), tends to diminish the effects of acoustic scattering in the solid skeleton of the granular packing.

For frequencies higher than the cut-off frequencies, the effect of diameter is more difficult to analyze. In average, for a smaller diameter, the transmission level is lower. This is expected from the equivalent fluid model, where air flow resistivity increases ($\sigma \propto d^{-2}$) and where characteristic thermal and viscous lengths decrease ($\Lambda' \propto \Lambda \propto d$) with decreasing diameter (complete formula of the equivalent fluid model for disordered granular media in air is given in Ref. 38).

Concerning the second harmonic generation, the picture is less clear. Figure 7 shows the second order FRFs for the three granular samples having different bead diameters. The noise level is -100 dB. The excitation amplitude corresponds to an acoustic deformation of 10^{-6}. The technique and set-up accuracy allows one to observe only the second harmonic signal when it is solid based in the low frequency region below the cut-off frequency f_c. This can be attributed to the fact that nonlinearity of the solid skeleton is much larger than nonlinearity of air (which has a parameter of quadratic nonlinearity of $\sim$1.2, i.e., at least three orders of magnitude lower than the nonlinear parameter of the granular skeleton). Together with a weak air-solid coupling and a quickly increasing attenuation in the solid skeleton as a function of frequency, it provides a much lower second harmonic level for frequencies above f_c compared to the low frequency region below f_c. Considering the noise level, it is not possible here to observe a second harmonic above 30 kHz in the best case.

The main difference observed when the bead diameter is modified is a higher level of the second harmonic for the smallest beads $d = 0.7$ mm. This is directly related to the higher level of fundamental wave at the origin of the second harmonic. However, there is no particular difference

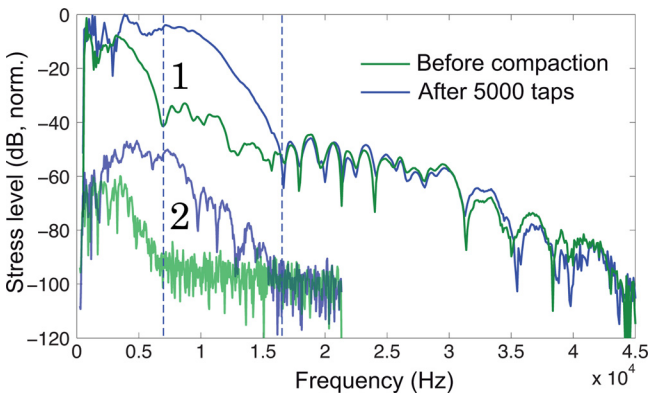

FIG. 6. (Color online) Received acoustic stress levels for the first and second order FRFs (indicated by 1 and 2, respectively). Curves before compaction and after the application of 5000 taps are presented. Glass beads are 0.7 mm in diameter. Curves are normalized to the maximum of the first order FRF with compaction.

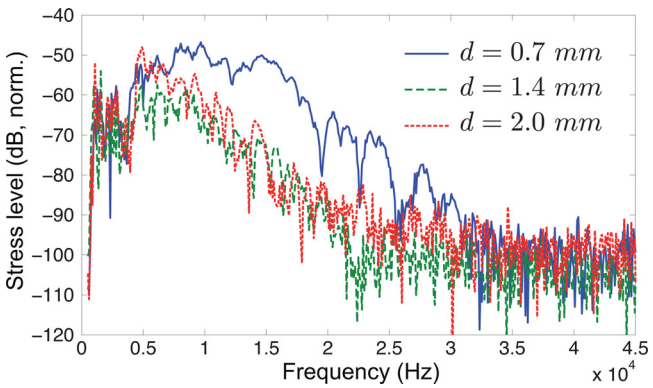

FIG. 7. (Color online) Received acoustic stress levels at the second harmonic frequency (second order FRF) for three granular samples composed of different bead diameters d. All three samples are compacted with 5000 taps. Curves are normalized to the maximum of the first order FRF for $d = 0.7$ mm.

between the two other bead diameters $d = 1.4$ mm and $d = 2$ mm.

E. Nonlinear self-action process

Other nonlinear or amplitude dependent effects have been observed on the first order FRF (i.e., at the fundamental excitation frequency). Such nonlinear manifestations are known as self-action effects.

In Fig. 8, the first and second order FRFs are plotted for increasing excitation level (−40, −36, −32, −28, −24, −20, −16, −12, and −8 dB), the maximum 0 dB corresponds to a 5 nm displacement of the emitter membrane at 10 kHz. For clarity, FRFs obtained for higher excitation levels are not shown because they overlap with the other ones. Focusing on the first order FRF, there are frequency regions where the received level increases constantly by steps of 4 dB, i.e., proportionally to the excitation level. It is the case, for instance, in the region 20–30 kHz. On the contrary, in the frequency region 10–17 kHz, the received level does not increase regularly and even can diminish as strong self-action effects occur.

In order to depict in a more visible way the self-action effects, the received acoustic stress are averaged over four different frequency bands for each excitation level. In Fig. 9, these averaged stresses are plotted as a function of the excitation level up to 0 dB.

For the three first frequency bands, chosen in the "solid controlled region" and in the frequency region of transition from solid controlled to fluid controlled regions, the nonlinear self-action effects are clearly observed—the received averaged stress level deviates from the linear increase denoted by the dashed lines. Still, for the three first frequency bands, the observed deviation from linear behavior is more and more important when the frequency increases. This can be partly explained by the increasing emitter efficiency with frequency, leading to larger excitation levels at high frequencies and thus more pronounced nonlinear effects. The observed self-action effect is particularly important for the frequency band 10−15 kHz close to the cut-off frequency. For instance, the received averaged stress level is less for an excitation level of −4 dB than for an excitation level of −25 dB. From previous considerations on the model

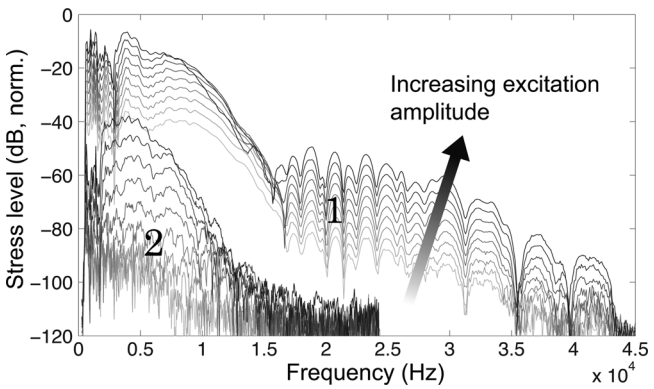

FIG. 8. Received acoustic stress levels for increasing excitation amplitudes at the fundamental frequency (indicated by 1) and at the second harmonic frequency (indicated by 2). The sample is composed of 0.7 mm in diameter glass beads and was submitted to 5000 taps.

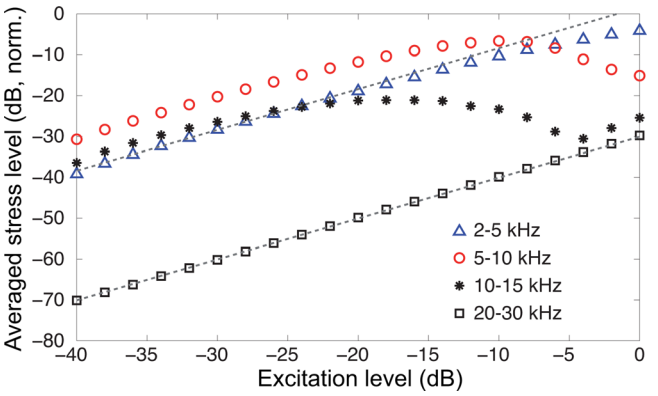

FIG. 9. (Color online) Received acoustic stress levels averaged over four different frequency bands (indicated in the figure) as a function of the excitation level. The reference 0 dB corresponds to a 5 nm displacement of the emitter membrane at 10 kHz. The raw data are those of the first order FRF of Fig. 8. The dashed lines show the linear dependence, i.e., an averaged stress level proportional to the excitation level.

and the analysis of the first order FRF, it is expected that scattering plays an important role in this frequency range. Consequently, the coexistence of strong nonlinear self-action effects and at the same time strong scattering, leads to the hypothesis that nonlinear scattering could occur at these frequencies. Nonlinear scattering can be seen as dynamic modifications of the complex propagation paths in the solid skeleton due to the acoustic wave itself.[52] Modifications can, in principle, be geometric (opening, closing of contacts for instance), due to average force variations (contact force).

In the "fluid controlled" region of the first order FRF, i.e., above the cut-off frequency $f_c \simeq 17$kHz, almost no self-action is observed. The received stress level behaves linearly as a function of the excitation level—the received averaged level between 20 and 30 kHz follows precisely the linear dependency. Most of the received acoustic energy propagates in this case through the fluid with a much lower nonlinearity than the solid skeleton.

Assuming a one-way plane wave propagating in the medium (which is justified by the rather strong attenuation in the medium evidenced by the absence of resonances above 5 kHz and in favor of nonlinear effects for one-way propagating waves), its amplitude evolution as a function of distance obeys the following equation:

$$\frac{\partial A}{\partial x} + \alpha(A)A = 0, \tag{10}$$

where $A(x)$ is the wave amplitude, and $\alpha(A)$ the amplitude-dependent attenuation coefficient. Equation (10) can be rewritten in the form

$$\frac{dA}{\alpha(A)A} = -dx. \tag{11}$$

Integrating this equation between the boundaries of the slab 0 and L, we obtain

$$\int_{A(0)}^{A(L)} \frac{dA'}{\alpha(A')A'} = -L. \tag{12}$$

Writing $A = A(L)$ and $A_0 = A(0)$, and differentiating Eq. (12) with respect to A_0 provides the following relation:

$$\frac{1}{\alpha(A)A}\frac{\partial A}{\partial A_0} - \frac{1}{\alpha(A_0)A_0} = 0, \tag{13}$$

which can be rewritten

$$\frac{\partial A}{\partial A_0} = \frac{\alpha(A)A}{\alpha(A_0)A_0} > 0. \tag{14}$$

The fact that the quantity $\partial A/\partial A_0$ is necessarily positive ensures that it is not possible to predict the observed effect in Fig. 9 of decreasing received amplitude A with increasing excitation amplitude A_0.

However, if we consider that the detected signal S (proportional to the total stress applied on the transducer membrane) is the sum of the stress in the solid σ_s and the stress in the fluid σ_f, we write

$$\bar{S} = A(A_0)e^{i(\omega t+\phi(A_0))} + BA_0e^{i\omega t}, \tag{15}$$

where $\bar{S}$ is the complex notation for S and A_0 is the excitation displacement amplitude. The first term of the right-hand side corresponds to the solid stress contribution with possible amplitude and phase nonlinear dependence on A_0 to account for nonlinear self-action and nonlinear softening of the medium. The second term of the right-hand side corresponds to the fluid stress contribution, which is supposed to behave linearly, with an amplitude proportional to A_0. The coefficient B accounts for the attenuation of the fluid stress wave in the medium over the distance L and for the solid-fluid impedance mismatch (the same excited acoustic displacement for the fluid and the solid at $x = 0$ leads to different solid and fluid excited stresses).

The main assumption in Eq. (15) is that the solid and the fluid waves are uncoupled in the medium, except at the transducer surface where the stresses are summed, and that there is no resonance in the slab. For the nonlinear self-action process in Fig. 9, the quantity of interest is

$$\frac{\partial|\bar{S}|}{\partial A_0} = \frac{\partial}{\partial A_0}\sqrt{A^2 + 2ABA_0\cos\phi + B^2A_0^2}, \tag{16}$$

$$\frac{\partial|\bar{S}|}{\partial A_0} = \frac{\dfrac{\partial(A^2)}{\partial A_0} + 2B\dfrac{\partial(AA_0\cos\phi)}{\partial A_0} + 2B^2A_0}{2(A^2 + 2ABA_0\cos\phi + B^2A_0^2)^{1/2}}, \tag{17}$$

$$\frac{\partial|\bar{S}|}{\partial A_0} = \frac{\dfrac{2\alpha A^2}{\alpha_0 A_0} + 2BA_0\left[\dfrac{\alpha A}{\alpha_0 A_0}\cos\phi + \dfrac{A}{A_0}\cos\phi - A\dfrac{\partial\phi}{\partial A_0}\sin\phi + B\right]}{2(A^2 + 2ABA_0\cos\phi + B^2A_0^2)^{1/2}}, \tag{18}$$

where $\alpha = \alpha(A)$ and $\alpha_0 = \alpha(A_0)$. In the general case, this expression for $\partial|\bar{S}|/\partial A_0$ is not necessarily positive unlike Eq. (14).

In particular, if the solid stress wave amplitude is close to saturation, i.e., $\partial A/\partial A_0 \simeq 0$, Eq. (17) can be rewritten as

$$\frac{\partial|\bar{S}|}{\partial A_0} = \frac{AB}{|\bar{S}|}\left[\frac{BA_0}{A} + \cos\phi + A_0\frac{\partial(\cos\phi)}{\partial A_0}\right]. \tag{19}$$

From Eq. (19), it follows that the most favorable conditions for the realization of the observed $\partial|\bar{S}|/\partial A_0 < 0$ in Fig. 9 could be $\cos\phi < 0$ and $\partial(\cos\phi)/\partial A_0 < 0$. It also seems from Eq. (19) that another favorable condition could be $A \gg BA_0$. However, the latter is not true because directly from Eq. (15) it follows that when $A \gg BA_0$, $|\bar{S}| \simeq A(A_0)$ and $\partial A/\partial A_0 \simeq \alpha A/\alpha_0 A_0 > 0$ as in Eq. (14). The received signal S exhibits a "classical" nonlinear self-action as for a single one-way wave. This is observed in Fig. 9 for the frequency band 2–5 kHz where the solid stress contribution dominates over the fluid one, i.e., when the condition $A \gg BA_0$ holds.

It also follows directly from Eq. (15), that in the opposite limiting case $A \ll BA_0$, the amplitude of the total signal is $|\bar{S}| \simeq BA_0$ and as a consequence $\partial A/\partial A_0 \simeq B > 0$. This is the case in Fig. 9 for the frequency band 20–30 kHz, where the fluid pressure contribution dominates ($A \ll BA_0$)—the received amplitude grows with the excitation amplitude and the process is linear.

It can be concluded that the adequate condition for the experimental realization of $\partial|\bar{S}|/\partial A_0 < 0$, and even of the oscillations in $|\bar{S}|$, is rather $A \sim BA_0$. For $A \simeq BA_0$ without assumption of the saturation of the amplitude $A(A_0)$, Eq. (18) leads to

$$\frac{\partial|\bar{S}|}{\partial A_0} \simeq B\left[\left(\frac{\alpha}{\alpha_0} + 1\right)\left|\cos\frac{\phi}{2}\right| - \mathrm{sign}\left(\cos\frac{\phi}{2}\right)\left(A\frac{\partial\phi}{\partial A_0}\right)\sin\frac{\phi}{2}\right]. \tag{20}$$

In this case, it is not obvious to extract the general behavior of $\partial|\bar{S}|/\partial A_0$, and its negative value is only ensured assuming peculiar inequalities for the amplitude rate change of the different terms.

Our experimental observations where $\partial|\bar{S}|/\partial A_0 < 0$ occur when the growth of A is saturated, while the continuous increase of A_0 leads the system to the transitional regime $A \sim BA_0$ (see the regime where the excitation amplitude A_0 is -20 to -15 dB for the detected stress in the frequency range 10–15 kHz in Fig. 9). When $A \simeq BA_0$ is substituted in Eq. (19), we obtain

$$\frac{\partial|\bar{S}|}{\partial A_0} \simeq \frac{B}{2|\cos\frac{\phi}{2}|}\left[1 + \cos\phi + A_0\frac{\partial}{\partial A_0}(\cos\phi)\right]. \tag{21}$$

As a consequence, the most favorable condition for the observation of $\partial|\bar{S}|/\partial A_0 < 0$ is $\phi \simeq \pi$, leading to the

minimization of $1+\cos\phi$ and to $\partial(\cos\phi)/\partial A_0 < 0$. Assuming that $\phi = \pi + \varepsilon$ ($|\varepsilon| \ll 1$), we transform Eq. (21) into the asymptotic form

$$\frac{\partial|\bar{S}|}{\partial A_0} \simeq B\left[\frac{|\varepsilon|}{2} + A_0\frac{\partial|\varepsilon|}{\partial A_0}\right]. \tag{22}$$

This result indicates that $\partial|\bar{S}|/\partial A_0 < 0$ is possible if the phase ϕ approaches the value π (corresponding to the anti-phase condition of the solid-based and fluid-based modes at the receiver) faster than $\propto 1/\sqrt{A_0}$, i.e., for instance, $|\phi-\pi| = |\varepsilon| \propto A_0^{-\gamma}$ with $\gamma > 1/2$. Considering hysteretic quadratic nonlinearity as the nonlinearity at the origin of the accumulated phase delay ϕ of the solid stress relative to the fluid stress (as shown from several previous studies on nonlinear softening for instance,[26,49] we have in this case $\partial\phi/\partial A_0 = C$, where C is a positive constant. Consequently, when $|\varepsilon|$ approaches 0, $\partial|\varepsilon|/\partial A_0 = -C$ and there is necessarily a small enough ε such that $|\varepsilon| < A_0 C$, providing $\partial|\bar{S}|/\partial A_0 < 0$ in Eq. (22).

Note that the same type of reasoning could hold for the interferences of a direct solid wave with scattered waves in the solid arriving with a relative phase delay, and the same qualitative effects could be expected. In this case, with increasing excitation amplitude, the nonlinear wave scattering would increase the phase delay and the scattered amplitude relative to the direct coherent wave.

These strong self-action effects on the fundamental frequency have influence on the efficiency of the second harmonic generation. A saturation mechanism for the second harmonic generation exists, and exhibits qualitatively the same frequency behavior as the self-action effect on the fundamental wave.

IV. SUMMARY

This analysis of the acoustic transmission through granular slabs under different conditions (compacity, bead diameter) has led to several observations and interpretations.

First, the acoustic transfer function of granular slabs can be qualitatively separated in different characteristic frequency bands—a low frequency band where the acoustic character of the propagation is mainly controlled by the properties of the solid skeleton of the bead packing (the bead and their contacts). In this case, the energy transports dominantly in the solid part of the granular medium. Above a cut-off frequency f_c, there is a second (middle) frequency band, where the acoustic propagation is mainly influenced by the "equivalent fluid" properties of the medium. The received energy in this case has dominantly been transported in the air saturating the beads. The third frequency band corresponds to the occurrence of scattering in the fluid, and the deviation from the equivalent fluid model.

The essential different behaviors of the solid controlled low frequency band and of the fluid controlled (equivalent fluid) middle frequency band are supported by the following consistent observations:

- The cut-off frequency f_c, interpreted to be mainly associated with the transmission drop associated to scattering in the solid skeleton, decreases with increasing bead diameter.
- The compaction process has a strong influence on the "solid controlled" frequency band (modification of the propagation paths, coordination number, static pressure, etc.).
- The compaction process has almost no influence on the "equivalent fluid" frequency band (equivalent fluid parameters only weakly depend on the compacity[38]).
- Nonlinear effects (second harmonic and importantly self-action) only occur in the "solid controlled" frequency band and are particularly marked when the solid stress amplitude approaches the fluid stress amplitude, just below f_c. No nonlinear effect has been observed in the "equivalent fluid" controlled frequency region due to the much lower nonlinearity of air compared to solid skeleton.

Second, the strong drop in transmitted level at frequencies just below the cut-off frequency f_c is found to be associated with scattering of the waves in the solid skeleton. This is also consistent with the above listed observations. The strong self-action effects observed in the frequency band 10–15 kHz (see Fig. 9) could be associated with nonlinear scattering by dynamic modifications of the propagation paths for the acoustic waves in the solid skeleton, nonlinear softening, and nonlinear dissipation together with the interferences on the receiver surface of the solid and fluid stresses. A developed qualitative model supports this idea and shows that necessary conditions for such observed strong self-action effects are the comparable amplitudes and opposite phases between solid stress and fluid stress at the receiver and nonlinear saturation of the solid stress wave.

Third, the comparison of the experimental results at the fundamental frequency and at the second harmonic frequency with the model[38] leads to the following conclusions. Except for the very low frequency part where the one-dimensional character of the model does not capture the possible experimental diffraction effects, a good agreement is obtain between the model and the experimental linear transfer functions. Only the elastic parameter of the solid skeleton is *a priori* unknown and has to be measured independently or adjusted. The measurement of the frequency dependent real and imaginary parts of the longitudinal elastic parameter of the solid skeleton is extremely complicated because of the several dependencies on experimental parameters (compaction step, bead diameter, static pressure, humidity, time, etc.). A whole characterization of this parameter would be highly desirable. A fair agreement is also observed for the second harmonic generation process. However, the model[38] does not account for the strong nonlinear self-action effects observed here experimentally.

We believe that this work sheds light on acoustic effects in granular media that can be of relevance for studies related to the acoustic probing of granular flows, avalanches, pre-avalanches,[53,54] surface waves on granular media,[55,56] and waves in nonlinear porous media. It also shows that air saturating a granular packing cannot, in the general case, be neglected, as it is often done.

ACKNOWLEDGMENTS

This study has been supported by ANR project "STABINGRAM'' ANR-2010-BLAN-0927-03. We acknowledge Claude Inserra for having initiated the observation of some of the effects reported here during his Ph.D. thesis.

[1]H. M. Jaeger and S. R. Nagel, "Physics of the granular state," Science **255**, 1523–1531 (1992).
[2]H. M. Jaeger, S. R. Nagel, and R. P. Behringer, "The physics of granular materials," Phys. Today **49**, 32–38 (1996).
[3]R. D. Mindlin and H. Deresiewicz, "Elastic spheres in contact under varying oblique forces," J. Appl. Mech. **20**, 327–344 (1953).
[4]K. L. Johnson, *Contact Mechanics* (Cambridge University Press, Cambridge, UK, 1985), pp. 1–452.
[5]C-H. Liu and S. R. Nagel, "Sound in sand," Phys. Rev. Lett. **68**, 2301–2304 (1992).
[6]C-H. Liu and S. R. Nagel, "Sound in a granular material: disorder and nonlinearity," Phys. Rev. B **48**, 15646–15650 (1993).
[7]C. S. O'Hern, L. E. Silbert, A. J. Liu, and S. R. Nagel, "Jamming at zero temperature and zero applied stress: The epitome of disorder," Phys. Rev. E **68**, 011306 (2003).
[8]H. A. Makse, N. Gland, D. L. Johnson, and L. Schwartz, "Granular packings: Nonlinear elasticity, sound propagation, and collective relaxation dynamics," Phys. Rev. E **70**, 061302 (2004).
[9]S. Job, F. Santibanez, F. Tapia, and F. Melo, "Nonlinear waves in dry and wet Hertzian granular chains," Ultrasonics **48**(6-7), 506–514 (2008).
[10]T. Brunet, X. Jia, and P. Mills, "Mechanisms for acoustic absorption in dry and weakly wet granular media," Phys. Rev. Lett. **101**(13), 138001 (2008).
[11]L. Bocquet, E. Charlaix, S. Ciliberto, and J. Crassous, "Moisture induced ageing in granular media," Nature **396**, 735–737 (1998).
[12]C.-J. Hsu, D. L. Johnson, R. Ingale, J. Valenza, N. Gland, and H. A. Makse, "Dynamic effective mass of granular media," Phys. Rev. Lett. **102**(5), 058001 (2009).
[13]M. A. Biot, "Theory of propagation of elastic waves in a fluid-filled-saturated porous solid," J. Acoust. Soc. Am. **28**, 168–191 (1956).
[14]M. A. Biot, "Mechanics of deformation and acoustic propagation in porous media," J. Appl. Phys. **33**(**4**), 1482–1498 (1962).
[15]J. F. Allard and N. Atalla, *Propagation of Sound in Porous Media: Modelling Sound Absorbing Materials*, 2nd ed. (Wiley, New York, 2009), pp. 1–358.
[16]M. J. Buckingham, "Wave propagation, stress relaxation, and grain-to-grain shearing in saturated, unconsolidated marine sediments," J. Acoust. Soc. Am. **108**, 2796–2815 (2000).
[17]R. D. Stoll, "Velocity dispersion in water-saturated granular sediment," J. Acoust. Soc. Am. **111**, 785–793 (2002).
[18]M. J. Buckingham, "On pore-fluid viscosity and the wave properties of saturated granular materials including marine sediments," J. Acoust. Soc. Am. **122**, 1486–1501 (2007).
[19]P. Richard, P. Philippe, F. Barbe, S. Bourles, X. Thibault, and D. Bideau, "Analysis by x-ray micro-tomography of a granular packing undergoing compaction,' Phys. Rev. E **68**, 020301 (2003).
[20]J.-F. Allard, M. Henry, J. Tizianel, L. Kelders, and W. Lauriks, "Sound propagation in air-saturated random packings of beads," J. Acoust. Soc. Am. **104**, 1–4 (1998).
[21]I. Y. Belyaeva, V. Y. Zaitsev, and E. M. Timanin, "Experimental study of nonlinear elastic properties of granular media with nonideal packing," Acoust. Phys. **40**, 789 (1994).
[22]X. Jia, C. Caroli, and B. Velicky, "Ultrasound propagation in externally stressed granular media," Phys. Rev. Lett. **82**, 1863–1866 (1999).
[23]V. Tournat, B. Castagnede, V. E. Gusev, and Ph. Béquin, "Self-demodulation acoustic signatures for non-linear propagation in glass beads," C. R. Mec. **331**, 119–125 (2003).
[24]V. Tournat, V. Yu. Zaitsev, V. E. Gusev, V. E. Nazarov, P. Béquin, and B. Castagnede, "Probing weak forces in granular media through nonlinear dynamic dilatancy: Clapping contacts and polarization anisotropy," Phys. Rev. Lett. **92**(8), 85502 (2004).
[25]V. Tournat, V. E. Gusev, and B. Castagnede, "Subharmonics and noise excitation in transmission of acoustic wave through unconsolidated granular medium," Phys. Lett. A **326**(5-6), 340–348 (2004).
[26]P. A. Johnson and X. Jia. Nonlinear dynamics, granular media and dynamic earthquake triggering," Nature **437**, 871–874 (2005).
[27]V. Tournat, V. Yu. Zaitsev, V. E. Nazarov, V. E. Gusev, and B. Castagnede, "Experimental study of nonlinear acoustic effects in a granular medium," Acoust. Phys. **51**(5), 543–553 (2005).
[28]V. Yu. Zaitsev, V. E. Nazarov, V. Tournat, V. Gusev, and B. Castagnede, "Luxembourg-Gorky effect in a granular medium: Probing perturbations of the material state via cross-modulation of elastic waves," Europhys. Lett. **70**(5), 607–613 (2005).
[29]S. R. Hostler and C. E. Brennen, "Pressure wave propagation in a granular bed," Phys. Rev. E **72**, 031303 (2005).
[30]K. Attenborough, "Models for the acoustical characteristics of air filled granular materials," Acta Acust. **1**, 213–226 (1993).
[31]K. V. Horoshenkov and J. Swift, "The acoustic properties of granular materials with pore size distribution close to log-normal," J. Acoust. Soc. Am. **110**, 2371–2378 (2001).
[32]G. Pispola, K. V. Horoshenkov, and F. Asdrubali, "Transmission loss measurement of consolidated granular media," J. Acoust. Soc. Am. **117**, 2716–2719 (2005).
[33]A. Moussatov, B. Castagnede, and V. Gusev, "Observation of nonlinear interaction of acoustic waves in granular materials: Demodulation process," Phys. Lett. A **283**, 216 (2001).
[34]M. Nicomedi, R. Delannay, P. Ribiere, D. Bideau, and P. Richard, "Slow relaxation and compaction of granular systems," Nature Mat. **4**, 121 (2005).
[35]C. Josserand, A. V. Tkachenko, D. M. Mueth, and H. M. Jaeger, "Memory effects in granular materials," Phys. Rev. Lett. **85**, 3632–3635 (2000).
[36]D. M. Mueth, H. M. Jaeger, and S. R. Nagel, "Force distribution in a granular medium," Phys. Rev. E **57**, 3164–3169 (1998).
[37]C. Inserra, V. Tournat, and V. E. Gusev, "Characterization of granular compaction by nonlinear acoustic resonance method," Appl. Phys. Lett **92**, 191916 (2008).
[38]O. Dazel and V. Tournat, "Nonlinear biot waves in porous media with application to unconsolidated granular media," J. Acoust. Soc. Am. **127**, 692–702 (2010).
[39]A. Novak, L. Simon, F. Kadlec, and P. Lotton, "Nonlinear system identification using exponential swept-sine signal," IEEE Trans. Instrum. Meas. **59**(8), 2220–2229 (2010).
[40]A. Novak, M. Bentahar, V. Tournat, R. El Guerjouma, and L. Simon, "Nonlinear acoustic characterization of micro-damaged materials through higher harmonic resonance analysis," NDT & E Int. **45**, 1–8 (2012).
[41]A. Farina, "Nonlinear convolution: A new approach for the auralization of distorting systems," in *Audio Engineering Society 108th Convention*, Amsterdam (2001).
[42]D. M. Donskoy, K. Khashanah, and T. G. McKee, Jr., "Nonlinear acoustic waves in porous media in the context of Biot's theory," J. Acoust. Soc. Am. **102**, 2521–2528 (1997).
[43]O. Dazel, B. Brouard, C. Depollier, and S. Griffiths, "An alternative Biot's displacement formulation for porous materials," J. Acoust. Soc. Am. **121**, 3509–3516 (2007).
[44]C. Coste, E. Falcon, and S. Fauve, "Solitary waves in a chain of beads under hertz contact," Phys. Rev. E **56**, 6104–6117 (1997).
[45]C. Coste and B. Gilles, "On the validity of hertz contact law for granular material acoustics," Eur. Phys. J. B **7**, 155–168 (1999).
[46]V. Tournat, V. E. Gusev, and B. Castagnede, "Self-demodulation of elastic waves in a 1D granular chain," Phys. Rev. E **70**, 056603 (2004).
[47]C. Coste and B. Gilles, "Sound propagation in a constrained lattice of beads: High-frequency behavior and dispersion relation," Phys. Rev. E **77**, 021302 (2008).
[48]N. Xu, V. Vitelli, M. Wyart, A. Liu, and S. Nagel, "Energy transport in jammed sphere packings," Phys. Rev. Lett. **102**(3), 038001 (2009).
[49]M. J. Buckingham, "Compressional and shear wave properties of marine sediments: Comparisons between theory and data," J. Acoust. Soc. Am. **117**, 137–152 (2005).
[50]V. Tournat, V. E. Gusev, V. Yu. Zaitsev, and B. Castagnede, "Acoustic second harmonic generation with shear to longitudinal mode conversion in granular media," Europhys. Lett. **66**(6), 798–804 (2004).
[51]V. Tournat and V. E. Gusev, "Acoustics of unconsolidated 'model' granular media: An overview of recent results and several open problems," Acta Acust. Acust. **96**, 208–224 (2009).
[52]V. Tournat and V. E. Gusev, "Nonlinear effects for coda-type elastic waves in stressed granular media," Phys. Rev. E **80**, 011306 (2009).

[53]V. Yu. Zaitsev, P. Richard, R. Delannay, V. Tournat, and V. E. Gusev, "Pre-avalanche structural rearrangements in the bulk of granular medium: Experimental evidence," EPL **83**, 64003 (2008).
[54]S. Kiesgen de Richter, V. Y. Zaitsev, P. Richard, R. Delannay, G. Le Caer, and V. Tournat, "Experimental evidence of ageing and slow restoration of the weak-contact configuration in tilted 3D granular packings," J. Stat. Mech.: Theory Exp. **2010**, P11023.
[55]X. Jacob, V. Aleshin, V. Tournat, P. Leclaire, W. Lauriks, and V. Gusev, "Acoustic probing of the jamming transition in an unconsolidated granular medium," Phys. Rev. Lett. **100**, 158003 (2008).
[56]L. Bonneau, B. Andreotti, and E. Clement, "Evidence of Rayleigh–Hertz surface waves and shear stiffness anomaly in granular media," Phys. Rev. Lett. **101**(11), 118001 (2008).